

# 1 European sulphate aerosols were a key driver of the early 2 twentieth-century intensification of the Asian summer monsoon

3  
4 Weihao Sun<sup>1,2</sup>, Massimo A. Bollasina<sup>1</sup>, Ioana Colfescu<sup>3,4</sup>, Guoxiong Wu<sup>2</sup> and Yimin Liu<sup>2</sup>

5  
6 <sup>1</sup>~~School of GeoSciences, University of Edinburgh, Edinburgh, UK~~[East China Sea Forecasting and Disaster  
7 Reduction Center, Ministry of Natural Resources, Shanghai, China](#)

8 <sup>2</sup>~~Key Laboratory of Earth System Numerical Modelling and Application, Institute of Atmospheric Physics,  
9 Chinese Academy of Sciences, Beijing, China.~~[Observation and Research Station of Huaniaoshan East China Sea  
10 Ocean-Atmosphere Integrated Ecosystem, Ministry of Natural Resources, Shanghai, China](#)

11 <sup>3</sup>School of Mathematics and Statistics, University of St Andrews, St Andrews, UK

12 <sup>4</sup>National Centre for Atmospheric Science, UK

13  
14  
15 Correspondence to: Massimo A. Bollasina ([Massimo.Bollasina@ed.ac.uk](mailto:Massimo.Bollasina@ed.ac.uk))

16  
17  
18 **Abstract.** Observations show that the Asian summer monsoon experienced substantial multi-decadal changes  
19 during the early 20<sup>th</sup> century, including a wetting trend over South Asia and a southward rainfall shift over East  
20 Asia. Despite their significance, these variations have received limited attention, and the underlying mechanisms  
21 remain poorly understood. This study investigates the role of increased European sulphate aerosol emissions in  
22 shaping these monsoon changes using ensemble experiments with the Community Earth System Model. The  
23 aerosol-driven rainfall patterns over South and East Asia resemble observations, suggesting that European  
24 aerosols played an important role in modulating the monsoon. These changes are linked to large-scale anomalies  
25 in surface climate and three-dimensional atmospheric circulation across the Indo-Pacific, which alter moisture  
26 transport to the continent, the main driver of the rainfall anomalies. Regional circulation anomalies form part of a  
27 hemispheric upper-tropospheric wave train originating over central Europe and extending through the Middle East  
28 to the Pacific. The wave train arises as a thermodynamic adjustment to the aerosol-induced surface cooling and  
29 related anticyclone over Europe, extends to the upper troposphere, and, while propagating eastward, induces three-  
30 dimensional circulation anomalies across Asia that affect the monsoon. These findings provide compelling  
31 evidence for the influence of European sulphate aerosols on the early 20<sup>th</sup>-century monsoon variability, which is  
32 relevant for improving current understanding of the regional-scale impacts of anthropogenic aerosols. As  
33 European SO<sub>2</sub> emissions continue to decline, this study sheds light upon a possible ongoing and future pathway  
34 which may significantly modulate the monsoon response to Asian aerosol changes.

35 **1 Introduction**

36 The Asian summer monsoon (ASM) is a vital source of water for over 60% of the world's population (Turner and  
37 Annamalai, 2012). Its interannual variability and long-term changes have significant implications for water  
38 resources, agriculture, and economic activities across Asia (e.g., Gadgil and Rupa Kumar, 2006).

39  
40 In the past decade, anthropogenic aerosols have attracted considerable scientific interest due to their ability to  
41 offset part of the warming caused by greenhouse gases (GHGs) (e.g., Samset et al., 2018; Hegerl et al., 2019; Li  
42 et al., 2022). Aerosols influence climate by scattering and absorbing solar radiation, and by acting as cloud  
43 condensation and ice nuclei, thereby modifying cloud albedo, lifetime, and precipitation processes (Boucher et  
44 al., 2013; Stier et al., 2024). They remain the largest source of uncertainty in estimating anthropogenic climate  
45 forcing since the pre-industrial era (Andrews and Forster, 2020; Bellouin et al., 2020). While their global historical  
46 effective radiative forcing is smaller than that of GHGs, aerosols can trigger strong regional climate responses due  
47 to their spatial and temporal variability (e.g., Szopa et al., 2021).

48  
49 The link between long-term changes in aerosol emissions and ASM variability is widely debated (e.g., Lau 2016;  
50 Li et al., 2016; Wu et al., 2016). Research is particularly challenging due to the compounding effects of internal  
51 variability, model biases, and divergent model responses (e.g., Saha and Gosh, 2019; Liu et al., 2024).  
52 Nonetheless, studies using observational and modelling evidence have highlighted the significant impact of  
53 aerosols, both regional (i.e., Asian-only) and remote (i.e., outside Asia), on the late 20<sup>th</sup> century weakening of the  
54 South ASM and the emergence of a southern-flood-northern-drought (SFND) pattern over East Asia (e.g.,  
55 Bollasina et al., 2011; Guo et al., 2013; Salzmann et al., 2014; Li et al., 2015; Dong et al. 2019; Wilcox et al.  
56 2020).

57  
58 Gauge records reveal clear multi-decadal variability in both South Asian and East Asian summer monsoons  
59 throughout the 20<sup>th</sup> century (e.g., Zhang and Zhou, 2011; Preethi et al., 2017; Li et al., 2023). In particular, the  
60 first half of the century saw an increase in rainfall over South Asia, most notably in central India, and a tripole  
61 pattern over East Asia, with excess rainfall in the south and northeast, and drier conditions along the Yangtze River  
62 basin. These anomalies appear to be part of a coherent ASM-wide fluctuation, mirrored in broader [Northern](#)  
63 [Hemispheric](#) summer monsoon changes (Zhang and Zhou, 2011; Preethi et al., 2017; Wang et al., 2018; Goswami

64 et al., 2023). Strikingly, this pattern reversed in the second half of the 20<sup>th</sup> century, producing comparable but  
65 opposite sign anomalies, and resulting in minimal net change over the full period.

66  
67 While monsoon changes since the 1950s have been extensively studied (e.g., Bollasina et al., 2011; Salzmann et  
68 al., 2014; Song et al., 2014; Liu et al., 2019; Liu et al., 2024; Shao et al., 2024), early-century variations have  
69 received less attention. Yet, given the contrasting trends throughout the historical period, understanding monsoon  
70 drivers and the underpinning physical mechanisms in the entire record is essential to constrain the nature of its  
71 multi-decadal variability and improve future projections. This is particularly relevant in the context of  
72 disentangling internal climate variability from externally-forced changes (e.g., Salzmann and Cherian, 2015;  
73 Huang et al., 2020). In this regard, compared to the later period, it is conceivable to assume a negligible role of  
74 Asian aerosols in the first half of the 20<sup>th</sup> century, as emissions underwent a significant growth only from the  
75 1950s and a sharp rise after the 1970s (Smith et al., 2011; Lund et al., 2019). In contrast, North American and  
76 European aerosols had already increased substantially, raising the possibility of their significant influence on the  
77 monsoon.

78  
79 Several studies have highlighted the potential role of remote, including European, aerosols in driving [Asian](#)  
80 [summer](#) monsoon changes (e.g., Cowan and Cai, 2011; Bollasina et al., 2014; Guo et al., 2015; Dong et al., 2016;  
81 Liu et al., 2018; Shawki et al., 2018; Undorf et al., 2018a,b; Westervelt et al., 2018; Wang et al., 2020). However,  
82 these analyses often relied on idealised simulations, such as long equilibrium experiments with present-day  
83 emissions turned on or off. Whether aerosol influences were already detectable in the early 20<sup>th</sup> century remains  
84 an open question. Addressing this gap is crucial for better understanding and narrowing uncertainty in aerosol-  
85 related future monsoon projections, especially considering divergent present-day emission trends (e.g., Wang et  
86 al., 2021a) and a wide range of plausible future pathways (Samset et al., 2019; Persad et al., 2023).

87  
88 Against this backdrop, this study investigates whether rising European sulphate aerosols – the dominant  
89 anthropogenic aerosol species of the region (e.g., Hoesly et al., 2018) – had any detectable impact on the ASM  
90 during the first half of the 20<sup>th</sup> century. Section 2 introduces the climate model, experimental setup, and  
91 observational data used. Section 3 presents the ASM response and examines the underlying mechanism.  
92 Discussion and conclusions are provided in Section 4.

## 94 **2 Data and methods**

95 The primary data comprises output from two transient historical (1850–2005) experiments with the fully coupled  
96 Community Earth System Model (CESM) version 1.2.2 (Hurrell et al., 2013). The atmospheric component is the  
97 Community Atmospheric Model version 5.3 (CAM5.3, Neale et al., 2012), which includes a 3-mode aerosol  
98 scheme and a prognostic representation of aerosol-cloud interactions (Ghan et al., 2012). The horizontal  
99 resolutions are  $1.9^\circ \times 2.5^\circ$  for the atmosphere and  $0.6^\circ \times 0.9^\circ$  for the ocean. The model reproduces spatial patterns  
100 and magnitude of the climatological summertime monsoon rainfall and low-tropospheric circulation reasonably  
101 well (Supplementary Fig-Figure S1), consistent with the overall performance of CMIP5/CMIP6 models (Meehl  
102 et al., 2020; He et al., 2023). A full description of the model and experiments is provided by Undorf et al. (2018a);  
103 here, we briefly summarise key details.

104

105 Each experiment consists of an 8-member ensemble initialised from different points in a 200-year pre-industrial  
106 (PI) simulation with fixed anthropogenic emissions at 1850 levels. The first experiment (ALL) includes time-  
107 varying historical emissions of anthropogenic aerosols, greenhouse gases, and natural forcing factors. The second  
108 (fixEU) is identical to ALL except that anthropogenic  $\text{SO}_2$  and  $\text{SO}_4$  emissions over Europe (EU) are held at PI  
109 levels. Europe is defined according to Tier 1 regions from the Hemispheric Transport of Air Pollution 2  
110 experiments (Koffi et al., 2016).

111

112 Several observational datasets are also used. Precipitation was taken from three land-only monthly gridded gauge-  
113 based datasets to account for uncertainties and discrepancies: the  $1^\circ \times 1^\circ$  Global Precipitation Climatology Centre  
114 v2020 (GPCC; Schneider et al., 2014), the  $0.5^\circ \times 0.5^\circ$  Climate Research Unit v4.00 (CRU; Harris et al., 2014),  
115 and the  $0.5^\circ \times 0.5^\circ$  University of Delaware v401 (UDEL, Willmott and Matsuura, 1995). Monthly sea level  
116 pressure surface is from the  $5^\circ \times 5^\circ$  Hadley Centre Sea Level Pressure dataset (HadSLP2; Allan and Ansell, 2006),  
117 and 850-hPa winds from the ECMWF Reanalysis 5 (Hersbach et al., 2020). Monthly observed precipitation from  
118 the  $2.5^\circ \times 2.5^\circ$  Climate Prediction Center Merged Analysis of Precipitation dataset (CMAP, Xie and Arkin, 2017)  
119 is also used for model validation.

120

121 The analysis focuses on the summer (June–August, JJA) monsoon variation during the early 20<sup>th</sup> century.  
122 Temporal changes are estimated using least-squares linear trends from 1901 to 1955. Alternative trend estimation  
123 methods (i.e., Sen’s non-parametric slope or differences between the 1941–1955 and 1901–1915 means) yield  
124 similar results (not shown). As the main objective is to isolate the influence of external forcing, particularly  
125 anthropogenic aerosols, on the ASM, changes are primarily assessed using ensemble means. Assuming linear  
126 additivity of responses, the difference between the ALL and fixEU experiments is interpreted as the impact of  
127 European SO<sub>2</sub> emissions. Statistical significance is assessed using a two-tailed Student’s *t*-test at the 90%  
128 confidence level. To identify the contribution of the model’s internal variability to the forced response, individual  
129 ensemble members are also examined. Additionally, the PI simulation is used to assess the statistical significance  
130 of the forced changes relative to internal variability. We generate 10,000 bootstrap samples of 8-member ensemble  
131 means to construct the probability distribution of unforced linear trends; the 90% confidence interval is defined  
132 as the range within which 90% of these fall.

### 133 3 Results

#### 134 3.1 Observed and simulated precipitation trends

135 Observational data show that JJA precipitation changes across Asia during the first half of the twentieth century  
136 exhibit a coherent large-scale pattern (Fig. Figure 1a), with robust features across multiple datasets  
137 (Supplementary Fig. Figure S2). Over South Asia, significant wetting is observed across central and northern  
138 India, contrasted by drying over southern and northeastern India, the eastern Himalayas and northern Myanmar.  
139 Further east, rainfall deficits occur over southern Indochina and Indonesia, with a pronounced drying over the  
140 middle and lower reaches of the Yangtze River valley (105°–120°E, 25°–35°N). In contrast, precipitation increases  
141 are seen in a band extending from northern Indochina through southern China, and further north into northwestern  
142 China and the Korean peninsula. Interestingly, the anomalous rainfall pattern over South Asia closely resembles,  
143 but with opposite sign, that associated with the late 20<sup>th</sup> century weakening of the monsoon, while the anomalies  
144 over eastern Asia are reminiscent of the reversed SFND pattern (e.g., Bollasina et al., 2011; Dong et al., 2016).

145

146 To provide further context on the long-term precipitation variations, Figure 1c shows the observed time series of  
147 monsoon rainfall anomalies over the core Indian monsoon region (75°–87°E, 16°–27°N land-only points, see box  
148 in Fig. Figure 1c). Beyond interannual and decadal fluctuations, the record reveals a marked increase from the

149 1900s to the mid–1950s (+0.55/+0.76 mm day<sup>-1</sup> in GPCP/CRU over 55 years, statistically significant at the 90%  
150 confidence level), equivalent to about 7–11% of the long-term climatology. The anomaly also results in a 5–7%  
151 increase in the All–India rainfall relative to early–century values. A similar analysis over southern China (110°–  
152 120°E, 25°–35°N; Supplementary Fig-Figure S3) also shows a prominent, statistically significant, multi-decadal  
153 trend.

154

155 Despite its coarser resolution, the ALL ensemble mean captures the main spatio-temporal characteristics of the  
156 observed precipitation trends, although amounts are generally smaller (Fig-Figure 1b). The model reproduces the  
157 observed widespread precipitation increase over northern India, albeit with a weaker magnitude (+0.14 mm day<sup>-1</sup>  
158 (55 years)<sup>-1</sup> over the core region) and a slight eastward shift, and the drying over southern India. The model likely  
159 underrepresents the full extent of the interaction with the Western Ghats. The simulated rainfall dipole over eastern  
160 China aligns with observations, although the amounts are slightly underestimated. However, the model fails to  
161 reproduce the observed wetting over southern China and northern Indochina, possibly due to limitations in  
162 resolving interactions with the complex terrain. The sign of the core precipitation anomalies over India is  
163 consistent across most of the individual ensemble members (6 out of 8), supporting a dominant anthropogenic  
164 origin (Supplementary Fig-Figure S4).

165

166 Preventing European sulphate aerosols from increasing results in drier conditions over central-northern India and  
167 the northern Bay of Bengal (BoB), with wetting over the eastern Himalayas and Myanmar. Concurrently, the  
168 precipitation anomalies over eastern Asia reverse polarity, while a pronounced precipitation deficit appears over  
169 Indochina. As a result, the precipitation pattern associated with increased European SO<sub>2</sub> emissions closely  
170 resembles observations and shows greater similarity than ALL across Asia. The aerosol-related precipitation  
171 response is also robust across most of the ensemble members (Supplementary Fig-Figure S4). For example, the  
172 ensemble-mean rainfall trend over the core Indian region amounts to +0.33 mm day<sup>-1</sup> over 55 years, with increases  
173 in 6 out of 8 ensemble members. This indicates that European aerosols substantially contributed to the early 20<sup>th</sup>-  
174 century ASM rainfall trends.

175

176 The observed and simulated 55-year rainfall trends over central-northern India are also compared with the  
177 corresponding range of trends from the PI experiment (Supplementary Figures. S4) and S5). The trend from CRU

178 is outside the respective 90% confidence interval, while it is slightly below in GPCC. The trend from the ALL-  
179 ensemble mean is within the corresponding 90% confidence interval (+0.19 mm day<sup>-1</sup> over 55 years;  
180 [Supplementary Figure S5](#)), although five of its members exhibit positive trends that are markedly discernible from  
181 internal variability. The ensemble-mean drying trend in the fixEU experiment exceeds the 90% confidence level.  
182 As a result, the ensemble-mean trend associated with European aerosols (EU) is clearly distinguishable from  
183 internally-generated fluctuations, even exceeding the 95% confidence level (+0.24 mm day<sup>-1</sup> over 55 years).

### 184 3.2 Changes in the monsoon circulation

185 Changes in precipitation across Asia are closely linked with variations in near-surface and atmospheric circulation  
186 patterns ([Fig-Figure 2](#)). The spatial correspondence between wet (dry) anomalies and regions of moisture flux  
187 convergence (divergence) underscores the dominant role of circulation-induced moisture transport in shaping  
188 monsoon precipitation trends ([Fig-Figure 2b](#)). Over South Asia, a prominent anomalous anticyclone centred over  
189 southern India and the western BoB characterises the low-tropospheric flow. Over East Asia and the western  
190 Pacific, a zonal dipole emerges: an anomalous cyclone spans northern Indochina, southeastern China, and the  
191 South China Sea, accompanied by an elongated anticyclone extending from central China to the western Pacific.

192  
193 As Figure 2a shows, strong low-level easterlies across southern India oppose the climatological westerlies from  
194 the Arabian Sea, leading to local rainfall deficits. Meanwhile, the climatological moisture-laden southwesterlies  
195 are deflected northward over the northern Arabian Sea. Upon reaching central and northern India, this flow  
196 converges with anomalous northeasterlies from northern Indochina and the northern BoB, enhancing rainfall ([Fig-](#)  
197 [Figure 2b](#)). On the western flank of the anomalous Indo-Pakistan low, dry northerlies suppress precipitation over  
198 Pakistan. Over East Asia, enhanced Pacific moisture transport into southern China and northeastern Indochina,  
199 opposing the climatological southerlies linked to the western Pacific subtropical high, leads to regional wetting.  
200 Return westerlies south of the anomalous Pacific low further reinforce the moisture flux from the BoB,  
201 contributing to widespread wetting across the Bay and northwestern Indochina. In contrast, reduced southerly  
202 moisture advection brings drying to southern Indonesia and northeastern China.

203  
204 Figure 2c shows that the regional upper-tropospheric circulation also exhibits substantial changes, consistent with  
205 the tropical balance among convective heating, ascent, and upper-level divergence (and vice versa). Over northern  
206 India and the northern BoB, strong mid-tropospheric ascent coincides with rainfall enhancement, accompanied by

207 divergent outflow in the upper troposphere. One branch heads northeastward, converging and subsiding over  
208 Burma and central China. Other branches are directed southwestward and southward, with corresponding mid-  
209 tropospheric subsidence and surface anticyclones over southern India and the northern equatorial Maritime  
210 Continent. A meridional system of divergent cells over East Asia and the western Pacific reflects the deep  
211 convection and upper-tropospheric divergence centred near 20°N. The southern cell also converges and subsides  
212 over the north equatorial Maritime Continent, aligning with the southern outflow from South Asia.

### 213 3.3 Aerosol forcing over Europe

214 To elucidate the generating mechanism, Figure 3a shows the widespread sulphate loading anomaly over Europe  
215 resulting from enhanced emissions. Once emitted, aerosols are transported across and beyond the Continent.  
216 Notably, aerosols spread southwestward towards northern Africa and the tropical Atlantic via the summertime  
217 climatological circulation of the Azores high, and eastward over central Eurasia by the midlatitude climatological  
218 westerlies, displacing the maximum loading and [Aerosol Optical Depth \(AOD\)](#) (~~Supplementary Figure S6~~  
219 ~~shown~~) eastward of the emissions source.

220  
221 Consistent with this transport, surface clear-sky downward shortwave radiation decreases across Europe, with  
222 anomalies exceeding  $-3 \text{ W m}^{-2}$  over 55 years in regions of peak aerosol loading (~~Fig-Figure~~ 3b), accounting for  
223 approximately 80% of the local reduction in the all-sky radiation (Supplementary ~~Fig-Figure~~ S6). All-sky  
224 radiation anomalies are larger (up to  $-5 \text{ W m}^{-2}$ ) due to increased cloudiness associated with circulation changes  
225 (see ~~last paragraph in this Section~~). As expected by the aerosol scattering effect, net shortwave differences  
226 between the top-of-atmosphere and surface are minimal (~~Supplementary Figure S6~~~~not shown~~). Including  
227 longwave effects, the net radiative cooling at the model top reached about  $-2 \text{ W m}^{-2}$  over central and eastern  
228 Europe (Supplementary ~~Figure~~: S6).

229  
230 Cloud droplet number concentration displays widespread positive anomalies over central and eastern Europe  
231 concurrently with a negative, albeit weak, decrease in cloud top effective radius (Supplementary ~~Fig-Figure~~ S6).  
232 These changes are consistent with those expected by the cloud response to sulphate aerosols, assuming negligible  
233 variations in water liquid content. The latter remains relatively unchanged or slightly enhanced due to anomalous  
234 northwesterlies from the Atlantic (see ~~next paragraph~~~~below~~).

235

236 As a result of the aerosol-induced dimming, near-surface temperature shows anomalous cooling over central and  
237 eastern Europe (Fig-Figure 3c), and concurrently, the circulation adjusts thermodynamically, with marked  
238 anticyclonic anomalies occurring at the surface. Interestingly, Fig-Figure 3d shows that the largest cooling and  
239 the high-pressure core are displaced east of the aerosol loading maximum, suggesting the combined influence of  
240 direct forcing, feedbacks, and modulation by the climatological flow. For example, eastward aerosol transport and  
241 temperature advection by the climatological westerlies contribute in concert to displacing the aerosol cooling to  
242 the east. The associated northeasterly flow on the eastern flank of the surface anticyclone further reinforces the  
243 cooling over eastern Europe. Note that the simulated northeastward displacement of the anomalous anticyclone is  
244 consistent with the displacement shown by pattern of observed sea-level pressure trends (Supplementary Fig-  
245 Figure S7).

#### 246 **3.4 Rossby wave propagation and remote teleconnections**

247 As shown in Figure 4, the regional signature of European aerosols extends to the mid and upper troposphere.  
248 Streamfunction anomalies feature a (weak) equivalent-barotropic nature and a slight northwestward tilt with  
249 height (not shown), consistent with the mature phase of an extratropical disturbance. At 300 hPa, anticyclonic  
250 anomalies are seen over central Europe. This pattern forms part of a wave train signal extending across the  
251 northern hemisphere, indicating a Rossby wave response to increased European aerosols and related upper-level  
252 relative vorticity anomalies, which serve as the primary source of wave activity.

253  
254 Upper-level meridional wind anomalies align with expectations from the streamfunction/geopotential height  
255 pattern, revealing alternating cyclonic and anticyclonic centres (Fig-Figure 4b). The wave activity flux (e.g.,  
256 Takaya and Nakamura 2001) highlights two eastward propagation branches. The main branch extends  
257 southeastward across the Middle East to Pakistan and northwestern India, where it weakens while turning  
258 northeastward into eastern China and converges over Japan. This flux follows the Asian jet stream, which acts as  
259 a Rossby waveguide. A secondary, weaker high-latitude pathway is also evident: the wave flux points  
260 northeastward towards northern Russia, crosses northern Eurasia, and then turns southeastward over the  
261 northwestern Pacific, ultimately converging with the main pathway.

262  
263 Mid-tropospheric ascent and descent anomalies accompany the wave train (Fig-Figure 4b), consistent with the  
264 vorticity balance (e.g., Rodwell and Hoskins 2001). For example, the anticyclonic anomaly over Afghanistan and

265 Pakistan induces southward flow and subsidence to its east, suppressing precipitation over Pakistan and the  
266 western Tibetan Plateau. Conversely, an anomalous upper-tropospheric anticyclone develops over eastern China  
267 and the western Pacific (120°-140°E). Northward flow and ascent occur on its western flank, while subsidence is  
268 found to the east, in agreement with the fundamental vorticity balance. At lower levels, this configuration  
269 generates an anomalous westerly flow from the western Pacific toward south-eastern China, enhancing moisture  
270 transport and producing a positive precipitation anomaly. This rainfall anomaly, in turn, drives strong variations  
271 in the tropical divergent circulation: part of the divergent outflow extends toward the Maritime Continent, where  
272 it converges, descends, and produces anomalous anticyclonic flow. The interaction between extratropical wave-  
273 induced anomalies over eastern China/western Pacific and the resulting meridional adjustments in the tropical  
274 divergent circulation account for the characteristic tripolar anomalous rainfall pattern across East Asia, over  
275 southern China, near-surface low-pressure anomalies, upward motion, and increased precipitation are associated  
276 with northward flow. These results suggest that key upper-tropospheric action centres, over the Middle East and  
277 southern China/western Pacific, initiate low-tropospheric circulation adjustments that generate the anomalous  
278 rainfall pattern across Asia.

#### 279 **4 Discussion and concluding remarks**

280 The Asian summer monsoon hydroclimate underwent significant changes in the early 20<sup>th</sup> century, characterised  
281 by a wetting trend over South Asia and a southern rainfall shift over East Asia. This study finds that increased  
282 European anthropogenic sulphate aerosols played a key role in driving these observed monsoon changes. The  
283 aerosol-induced cooling and large-scale anticyclonic anomaly over central/eastern Europe extend from the surface  
284 to the upper troposphere. These anomalies trigger subsequent atmospheric circulation adjustments in the form of  
285 an eastward propagating Rossby-wave train, which is central to realising the remote aerosol impact across Asia.

286  
287 These findings shed new light on the drivers and mechanisms of monsoon multidecadal variability. While most  
288 existing research has focused on recent monsoon changes, the early historical period remains unexplored.  
289 Moreover, many prior studies have relied on long, equilibrium-type experiments to enhance the signal-to-noise  
290 ratio, but these are less representative of the transient response to evolving aerosol emissions. An atmospheric  
291 propagation pathway similar to the one identified here has been discussed in earlier literature, particularly in  
292 relation to the downstream signature of the North Atlantic Oscillation (e.g., Watanabe 2004) and broader

293 teleconnections between Europe and East Asia (e.g., Lu et al. 2002; Enomoto et al., 2003), yet it has been largely  
294 overlooked in the context of aerosol forcing (e.g., Wang et al., 2021b), which has instead typically emphasised  
295 changes in the large-scale meridional temperature gradient across Eurasia as the dominant key mechanism.

296

297 Placing our study within the broader literature on remote aerosol-monsoon interactions underscores its relevance.  
298 Cowan and Cai (2011) were among the first to identify the influence of non-Asian aerosols, primarily European  
299 sulphate, in weakening the ASM over the 20<sup>th</sup> century by inducing widespread Eurasian cooling and thereby  
300 reducing the meridional temperature gradient, which in turn weakens the southerly monsoon flow. Similarly, Guo  
301 et al. (2015, 2016) linked widespread drying across Asia to increased global aerosol emissions, mainly from non-  
302 Asian sources, and the subsequent modulation of the zonal-mean meridional temperature gradient. Focusing on  
303 the fast, atmospheric-only equilibrium response to the removal of European aerosols, Dong et al. (2016) reported  
304 a strengthening of the South Asian monsoon and a southern shift in East Asian rainfall, attributed to the  
305 downstream advection of cooler, drier air from Europe to Asia and consequent weakening of the tropospheric  
306 thermal gradient. Shawki et al. (2018) similarly found that removing European aerosol emissions strengthens,  
307 albeit weakly, the South Asian monsoon and shifts the East Asian monsoon northward, via changes in the large-  
308 scale temperature gradient and the interhemispheric heat and moisture transport. Liu et al. (2018) reported a slight  
309 decrease in annual mean precipitation over Asia associated with increased European sulphate aerosols, driven by  
310 the slow (ocean-mediated) component of the total response via inter-hemispheric heating redistribution. Similar  
311 rainfall patterns were also shown by Westervelt et al. (2018). More recently, Wang et al. (2017) and Wang et al.  
312 (2020) highlighted that non-local aerosol emissions are as influential as local ones in weakening the East Asian  
313 summer monsoon, primarily through easterly advection of colder air across Eurasia and resulting change in  
314 meridional heat transport, in agreement with Dong et al. (2016).

315

316 An enhanced meridional temperature gradient between central Eurasia and the IO is a well-known contributor to  
317 stronger monsoon precipitation over South Asia (e.g., Meehl and Arblaster, 2002). Indeed, this has been identified,  
318 for example, as one of the elements contributing to enhanced future monsoon precipitation by the end of the 21<sup>st</sup>  
319 century (e.g., Meehl et al., 2024). This outcome, however, is not borne out in our study, as the mid and high  
320 troposphere temperature averaged over the 60°-100°E sector displays enhanced cooling compared to the north-  
321 equatorial IO, resulting in a weaker meridional temperature gradient (not shown). This discrepancy indicates that

322 the aerosol-induced regional monsoon circulation and precipitation variations over South Asia cannot be explained  
323 by broad-scale sector-mean temperature changes. On the contrary, the anomalous temperature pattern over Eurasia  
324 displays a close relationship with that induced by the anomalies in atmospheric advection, especially in the  
325 meridional direction, in turn associated with the upper-tropospheric wave train.

326  
327 This dynamical pathway and the critical role of large-scale remotely driven atmospheric dynamical changes finds  
328 support in Bollasina et al. (2014). Although secondary to regional emissions in explaining the recent monsoon  
329 rainfall decline, extratropical aerosols were nonetheless shown to induce widespread temperature and wind  
330 anomalies across Asia, revealing the complex interplay between aerosol forcing, precipitation, and circulation  
331 changes. Undorf et al. (2018a, b) also highlighted the importance of midlatitude aerosol forcing in explaining the  
332 observed weakening of the South Asian monsoon through the mid-1970s, underscoring the key role of Eurasian-  
333 scale dynamical adjustments.

334  
335 An important question is whether Indian Ocean (IO) SSTs also influenced the monsoon. The ALL ensemble,  
336 consistent with the overall performance of CMIP5/6 models (e.g., Roxy et al., 2014), exhibits widespread and  
337 relatively homogeneous warming across the basin. In contrast, aerosol-induced SST trends, albeit weak, show  
338 warming over the western equatorial IO and cooling over the subequatorial regions (Supplementary Figure S8).  
339 This cross-equatorial dipole in SST trends is also evident, and more pronounced, in observations (e.g., Figure 3  
340 in Goswami et al., 2023), which suggests an aerosol contribution to the IO warming pattern. Further analysis of  
341 the EU ensemble (Supplementary Figure S8~~not shown~~), shows that SST anomalies are largely anticorrelated with  
342 evaporation: reduced evaporation dominates the western and equatorial IO, while increases are seen in the south.  
343 Concurrently, anomalous near-surface divergent easterlies across the north-equatorial IO oppose the  
344 climatological (south) westerlies, reducing evaporation and upwelling, which contribute to warming the SSTs.  
345 These patterns are similar to those associated with the Indian summer monsoon multi-decadal variability during  
346 the 20<sup>th</sup> century (Goswami et al., 2023). Also, the 55-year SST pattern resembles 20<sup>th</sup>-century-long changes,  
347 although the latter exhibits weaker anomalies and a less pronounced cooling (e.g., Rao et al., 2012; Roxy et al.,  
348 2014). Uncertainties remain in identifying the causes of the persistent western IO warming due to strong feedbacks  
349 between oceanic anomalies, atmospheric circulation, and convection (e.g., Rao et al., 2012; Swapna et al., 2014).  
350 While our findings highlight the role of remotely-forced wind anomalies, other mechanisms may also contribute.

351 While SST anomalies and rainfall are anticorrelated in the long term, this relationship reverses in the early 20<sup>th</sup>  
352 century (Fig. Figure 3 in Roxy et al., 2015), aligning with our findings.

353

354 Our results have important implications. They suggest that non-local anthropogenic aerosols have contributed  
355 significantly to shaping monsoon variability even during the early historical period. This is particularly relevant  
356 for understanding regional-scale impacts of anthropogenic forcing, which remain uncertain due to the spatial  
357 heterogeneity of emissions and their diverse climate effects. Importantly, under the current continued decrease in  
358 European aerosol emissions, assuming an opposite ASM response to the one described above, remotely-driven  
359 precipitation anomalies may significantly modulate, if not partially offset, the response to Asian aerosol emission  
360 changes (already declining or expected to do so in the future; e.g., Lund et al., 2019; Xiang et al. 2023). For  
361 example, assuming linearity in the combined responses, the abatement of EU sulphate aerosols would lead to a  
362 weaker monsoon over most of South Asia, and India in particular, which is opposite to the expected wetting  
363 associated with decreased sulphate aerosols over both South and East Asia (e.g., Bartlett et al., 2018). Conversely,  
364 EU aerosol reductions would contribute to further amplify the reversed SFND pattern over China brought about  
365 by decreased East Asian aerosol alone (e.g., Dong et al., 2016), resulting, for example, in enhanced drying over  
366 southeastern China. While the future monsoon response to the projected decline in worldwide aerosol emissions  
367 will most likely result from non-linear interactions among the different aerosol source regions, the above picture  
368 illustrates the complex interplay among local and remote aerosols and the need for a consistent and coordinated  
369 modelling and analysis approach (e.g., Wilcox et al., 2023).

370

371 While our analysis emphasises the central role of European aerosols, other remote emissions (e.g., from North  
372 America) and external forcings (e.g., greenhouse gases) may have also played a role. Our conclusions are based  
373 on ensemble experiments comprising eight members each, consistent with the minimum number typically  
374 recommended for detecting forced multi-decadal signals (e.g., Deser et al., 2012). However, internal variability  
375 cannot be ruled out, and studies have, for example, discussed the association of Atlantic slow-frequency variability  
376 with the ISM multi-decadal mode (e.g., Rajesh and Goswami, 2020). In this context, the use of large single-forcing  
377 ensembles (e.g., Smith et al., 2022; Simpson et al., 2023) offers a promising approach to disentangling the  
378 individual contributions of greenhouse gases, anthropogenic aerosols and other external drivers. Furthermore, our  
379 findings are based on a single climate model and therefore depend on its representation of aerosol-cloud-radiation

380 and circulation interactions. Given the well-known uncertainties in aerosol forcing and its climatic effects, the  
381 response may differ across models and from real-world observations. For example, CESM1 is known to exhibit a  
382 relatively strong aerosol effective radiative forcing (Zelinka et al., 2014; 2023), which may result in a stronger  
383 climate response to aerosol perturbations than seen in other models.

384

385 **Acknowledgements.** MAB acknowledges support from the Natural Environment Research Council  
386 (NE/N006038/1) and the Research Council of Norway (grant no. 324182; CATHY).

387

388 **Data availability.** GPCP data are retrieved from <https://psl.noaa.gov/data/gridded/data.gpcp.html>, CRU data from  
389 <https://crudata.uea.ac.uk/cru/data/hrg/>, and UDEL data from  
390 [https://psl.noaa.gov/data/gridded/data.UDEL\\_AirT\\_Precip.html](https://psl.noaa.gov/data/gridded/data.UDEL_AirT_Precip.html). The ERA5 data are obtained at  
391 <https://cds.climate.copernicus.eu/datasets/reanalysis-era5-pressure-levels-monthly-means>. HadISST data are  
392 available from <https://www.metoffice.gov.uk/hadobs/hadisst/>, while the HadSLP2 dataset is accessed from  
393 <https://www.metoffice.gov.uk/hadobs/hadslp2/>. The CESM model data used in this study are available from MAB  
394 upon request.

395

396 **Author contribution.** WS and MAB designed the study. WS performed the analysis and completed the first draft  
397 of the manuscript. WS and MAB discussed the results, WA, MAB, and IC edited the manuscript. GW and YL  
398 provided suggestions on the analysis and interpretation of the results.

399

400 **Competing interests.** The authors have no competing interests to declare.

401

402 **References**

- 403 Allan, R., and Ansell, T.: A New Globally Complete Monthly Historical Gridded Mean Sea Level Pressure Dataset  
404 (HadSLP2): 1850–2004, *J. Climate*, 19, <https://doi.org/10.1175/JCLI3937.1>, 2006.
- 405 Andrews, T., and Forster, P.M.: Energy budget constraints on historical radiative forcing, *Nat. Clim. Chang.* 10,  
406 <https://doi.org/10.1038/s41558-020-0696-1>, 2020.
- 407 Bartlett, R. E., Bollasina, M. A., Booth, B. B. B. et al.: Do differences in future sulfate emission pathways matter  
408 for near-term climate? A case study for the Asian monsoon, *Clim. Dynam.*, 50, [https://doi.org/10.1007/s00382-](https://doi.org/10.1007/s00382-017-3726-6)  
409 [017-3726-6](https://doi.org/10.1007/s00382-017-3726-6), 2018.
- 410 Bellouin, N., et al.: Bounding aerosol radiative forcing of climate change, *Rev. Geophys.*, 58,  
411 <https://doi.org/10.1029/2019RG000660>, 2020.
- 412 Bollasina, M.A, Ming, Y, Ramaswamy, V.: Anthropogenic aerosols and the weakening of the South Asian summer  
413 monsoon, *Science*, 334, <https://doi.org/10.1126/science.1204994>, 2011.
- 414 Bollasina, M. A., Ming, Y., Ramaswamy, V., Schwarzkopf, M. D., and Naik, V.: Contribution of local and remote  
415 anthropogenic aerosols to the twentieth century weakening of the South Asian monsoon, *Geophys. Res. Lett.*,  
416 41, <https://doi.org/10.1002/2013GL058183>, 2014.
- 417 Boucher, O., Randall, D., Artaxo, P., Bretherton, C., Feingold, G., Forster, P., Kerminen, V.-M., Kondo, Y., Liao,  
418 H., Lohmann, U., Rasch, P., Satheesh, S., Sherwood, S., Stevens, B., and Zhang, X.: Clouds and aerosols, in  
419 *Climate change 2013: The physical science basis. Contribution of Working Group I to the Fifth Assessment*  
420 *Report of the Intergovernmental Panel on Climate Change*, edited by Stocker T., Qin D., Plattner G.-K., Tignor  
421 M., Allen S., Boschung J., Nauels A., Xia Y., Bex V., and Midgley P., chap. 7, pp. 571–658, Cambridge  
422 University Press, Cambridge, United Kingdom and New York, NY, USA,  
423 <https://10.1017/CBO9781107415324.016>, 2013.
- 424 Cowan, T. and Cai, W.: The impact of Asian and non-Asian anthropogenic aerosols on 20th century Asian summer  
425 monsoon, *Geophys. Res. Lett.*, 38, <https://doi.org/10.1029/2011GL047268>, 2011.
- 426 Deser, C., Phillips, A., Bourdette, V., et al.: Uncertainty in climate change projections: the role of internal  
427 variability, *Clim. Dynam.*, 38, <https://doi.org/10.1007/s00382-010-0977-x>, 2012.
- 428 Dong, B., Sutton, R. T., Highwood, E. J., and Wilcox, L. J.: Preferred response of the East Asian summer monsoon  
429 to local and non-local anthropogenic sulphur dioxide emissions, *Clim. Dynam.*, 46,  
430 <https://doi.org/10.1007/s00382-015-2671-5>, 2016.

431 Dong, B., Wilcox, L.J., Highwood, E.J., and Sutton, R. T.: Impacts of recent decadal changes in Asian aerosols on  
432 the East Asian summer monsoon: roles of aerosol–radiation and aerosol–cloud interactions, *Clim. Dynam.*,  
433 53, <https://doi.org/10.1007/s00382-019-04698-0>, 2019.

434 Enomoto, T., Hoskins, B.J., and Matsuda, Y.: The formation mechanism of the Bonin high in August, *Q. J. Roy.*  
435 *Meteor. Soc.*, 129, <https://doi.org/10.1256/qj.01.211>, 2003.

436 Gadgil, S., and Rupa Kumar, K.: The Asian monsoon — agriculture and economy. In: *The Asian Monsoon*.  
437 Springer Praxis Books. Springer, Berlin, Heidelberg. [https://doi.org/10.1007/3-540-37722-0\\_18](https://doi.org/10.1007/3-540-37722-0_18), 2006.

438 Ghan, S. J., Liu, X., Easter, R. C., Zaveri, R., Rasch, P. J., et al.: Toward a minimal representation of aerosols in  
439 climate models: Comparative decomposition of aerosol direct, semidirect, and indirect radiative forcing, *J.*  
440 *Climate*, 25, <https://doi.org/10.1175/JCLI-D-11-00650.1>, 2012.

441 Goswami, D. J., Ashok, K., and Goswami, B. N.: Local ocean–atmosphere interaction in Indian summer monsoon  
442 multi-decadal variability, *Clim. Dynam.*, 60, <https://doi.org/10.1007/s00382-022-06377-z>, 2023.

443 Guo, L., Highwood, E. J., Shaffrey, L. C., and Turner, A. G.: The effect of regional changes in anthropogenic  
444 aerosols on rainfall of the East Asian summer monsoon, *Atmos. Chem. Phys.*, 13, [https://doi.org/10.5194/acp-](https://doi.org/10.5194/acp-13-1521-2013)  
445 [13-1521-2013](https://doi.org/10.5194/acp-13-1521-2013), 2013.

446 Guo, L., Turner, A. G., and Highwood, E. J.: Impacts of 20<sup>th</sup> century aerosol emissions on the South Asian  
447 monsoon in the CMIP5 models, *Atmos. Chem. Phys.*, 15, <https://doi.org/10.5194/acp-15-6367-2015>, 2015.

448 Harris, I., Jones, P.D., Osborn, T.J. and Lister, D.H.: Updated high-resolution grids of monthly climatic  
449 observations – the CRU TS3.10 Dataset, *Int. J. Climatol.*, 34, <https://doi.org/10.1002/joc.3711>, 2014.

450 He, L., Zhou, T., and Chen, X.: South Asian summer rainfall from CMIP3 to CMIP6 models: biases and  
451 improvements, *Clim. Dynam.*, 61, <https://doi.org/10.1007/s00382-022-06542-4>, 2023.

452 Hegerl G.C., Bronnimann S., et al.: Causes of climate change over the historical record, *Environ. Res. Lett.*, 14,  
453 <https://doi:10.1088/1748-9326/ab4557>, 2019.

454 Hersbach, H., Bell, B., Berrisford, P., et al.: The ERA5 global reanalysis. *Q. J. Roy. Meteor. Soc.*, 146,  
455 <https://doi.org/10.1002/qj.3803>, 2020.

456 Hoesly, R.M., et al.: Historical (1750–2014) anthropogenic emissions of reactive gases and aerosols from the  
457 Community Emissions Data System (CEDS), *Geosci. Model Dev.*, 11, [https://doi.org/10.5194/gmd-11-369-](https://doi.org/10.5194/gmd-11-369-2018)  
458 [2018](https://doi.org/10.5194/gmd-11-369-2018), 2018.

459 Huang, X., and Coauthors: The recent decline and recovery of Indian summer monsoon rainfall: relative roles of

460 external forcing and internal variability, *J. Climate*, 33, <https://doi.org/10.1175/JCLI-D-19-0833.1>, 2020.

461 Hurrell, J. W., Holland, M. M., Gent, P. R., Ghan, S., Kay, J. E., et al.: The Community Earth System Model, *Bull.*  
462 *Amer. Met. Soc.*, 94, <https://doi.org/10.1175/BAMS-D-12-00121.1>, 2013.

463 Koffi, B., Dentener, F., Janssens-Maenhout, G., Guizzardi, D., Crippa, M., et al.: Hemispheric transport air  
464 pollution (HTAP): Specification of the HTAP2 experiments ensuring harmonized modelling (Tech. rep.)  
465 Luxembourg: Joint Research Centre JRC. <https://doi.org/10.2788/725244>, 2016.

466 Lau, W.K.M.: The aerosol-monsoon climate system of Asia: A new paradigm, *J. Meteor. Res.*, 30,  
467 <https://doi.org/10.1007/s13351-015-5999-1>, 2016.

468 Li, X., Li, Q., Ding, Y., Yang, S., et al.: Possible influence of the interdecadal variation of the extratropical southern  
469 Indian Ocean SST on East Asian summer monsoon precipitation, *Atmos. Res.*, 288,  
470 <https://doi.org/10.1016/j.atmosres.2023.106721>, 2023.

471 Li, X., Ting, M., Li, C., and Henderson, N.: Mechanisms of Asian summer monsoon changes in response to  
472 anthropogenic forcing in CMIP5 models, *J. Climate*, 28, <https://doi.org/10.1175/JCLI-D-14-00559.1>, 2015.

473 Li, Z., et al.: Aerosol and monsoon climate interactions over Asia, *Rev. Geophys.*, 54,  
474 <https://doi.org/10.1002/2015RG000500>, 2016.

475 Li, J., Carlson, B.E., Yung, Y.L., et al.: Scattering and absorbing aerosols in the climate system, *Nat. Rev. Earth*  
476 *Environ.*, 3, <https://doi.org/10.1038/s43017-022-00296-7>, 2022.

477 Liu, L., Shawki, D., Voulgarakis, A., Kasoar, M., Samset, B. H., et al.: A PDRMIP Multimodel study on the  
478 impacts of regional aerosol forcings on global and regional precipitation, *J. Climate*, 31,  
479 <https://doi.org/10.1175/JCLI-D-17-0439.1>, 2018.

480 Liu, Y., Cai, W., Sun, C., Song, H., Cobb, K. M., et al.: Anthropogenic aerosols cause recent pronounced  
481 weakening of Asian summer monsoon relative to last four centuries, *Geophys. Res. Lett.*, 46, 5469–5479,  
482 <https://doi.org/10.1029/2019GL082497>, 2019.

483 Liu, Z., Bollasina, M. A., and Wilcox, L. J.: Impact of Asian aerosols on the summer monsoon strongly modulated  
484 by regional precipitation biases, *Atmos. Chem. Phys.*, 24, 7227–7252, [https://doi.org/10.5194/acp-24-7227-](https://doi.org/10.5194/acp-24-7227-2024)  
485 [2024](https://doi.org/10.5194/acp-24-7227-2024), 2024.

486 Lu, R.-Y., Oh, J.H., and Kim, B.J.: A teleconnection pattern in upper-level meridional wind over the North African  
487 and Eurasian continent in summer, *Tellus A*, 54, <https://doi.org/10.3402/tellusa.v54i1.12122>, 2002.

488 Lund, M. T., Myhre, G., and Samset, B. H.: Anthropogenic aerosol forcing under the Shared Socioeconomic

489 Pathways, Atmos. Chem. Phys., 19, <https://doi.org/10.5194/acp-19-13827-2019>, 2019.

490 Meehl, G. A., and Arblaster, J. M.: GCM sensitivity experiments for the Indian monsoon and tropospheric biennial  
491 oscillation transition conditions, J. Climate, 15, [https://doi.org/10.1175/1520-0442\(2002\)015<0923:imgset>2.0.co;2](https://doi.org/10.1175/1520-0442(2002)015<0923:imgset>2.0.co;2), 2002.

492

493 Meehl, G.A., Shields, C., Arblaster, J.M., Annamalai, H., and Neale, R.: Intraseasonal, seasonal, and interannual  
494 characteristics of regional monsoon simulations in CESM2, J. Adv. Model. Earth Sys., 12,  
495 <https://doi.org/10.1029/2019MS001962>, 2020.

496 Meehl, G. A., Shields, C. A., Arblaster, J. M., Fasullo, J., Rosenbloom, N., Hu, A., et al.: Processes that contribute  
497 to future South Asian monsoon differences in E3SMv2 and CESM2, Geophys. Res. Lett., 51,  
498 <https://doi.org/10.1029/2024GL109056>, 2024.

499 Neale, R. B., Gettelman, A., Park, S., Chen, C.-C., Lauritzen, P. H., et al.: Description of the NCAR Community  
500 Atmosphere Model (CAM 5.0), NCAR technical note, NCAR/TN-48, 274.  
501 <https://doi.org/10.5065/D6N877R0>, 2012.

502 Persad, G., Samset, B.H., Wilcox, L.J., Allen, R.J., Bollasina, M.A., et al.: Rapidly evolving aerosol emissions are  
503 a dangerous omission from near-term climate risk assessments, Environ. Res. Climate, 2,  
504 <https://doi.org/10.1088/2752-5295/acd6af>, 2023.

505 Preethi, B., Mujumdar, M., Kripalani, R.H. et al.: Recent trends and tele-connections among South and East Asian  
506 summer monsoons in a warming environment, Clim. Dynam., 48, <https://doi.org/10.1007/s00382-016-3218-0>, 2017.

507

508 Rajesh, P. V., and Goswami, B. N.: Four-dimensional structure and sub-seasonal regulation of the Indian summer  
509 monsoon multi-decadal mode, Clim. Dynam., 55, <https://doi.org/10.1007/s00382-020-05407-y>, 2020.

510 Rao, S.A., Dhakate, A.R., Saha, S.K. et al.: Why is Indian Ocean warming consistently?, Climatic Change, 110,  
511 <https://doi.org/10.1007/s10584-011-0121-x>, 2012.

512 Rayner, N. A., Parker, D. E., Horton, E. B., Folland, C. K., Alexander, L. V., Rowell, D. P., Kent, E. C., and  
513 Kaplan, A.: Global analyses of sea surface temperature, sea ice, and night marine air temperature since the late  
514 nineteenth century, J. Geophys. Res., 108, <https://doi.org/10.1029/2002JD002670>, 2003.

515 Rodwell, M. J., and Hoskins, B. J.: Subtropical anticyclones and summer monsoons, J. Climate, 14,  
516 [https://doi.org/10.1175/1520-0442\(2001\)014<3192:SAASM>2.0.CO;2](https://doi.org/10.1175/1520-0442(2001)014<3192:SAASM>2.0.CO;2), 2001.

517 Roxy, M. K., Ritika, K., Terray, P., and Masson, S.: The curious case of Indian Ocean warming. J. Climate, 27,

518 <https://doi.org/10.1175/JCLI-D-14-00471.1>, 2014.

519 Roxy, M., Ritika, K., Terray, P. et al.: Drying of Indian subcontinent by rapid Indian Ocean warming and a  
520 weakening land-sea thermal gradient, *Nat. Commun.*, 6, <https://doi.org/10.1038/ncomms8423>, 2015.

521 Saha, A., and Ghosh, S.: Can the weakening of the Indian Monsoon be attributed to anthropogenic aerosols?  
522 *Environ. Res. Commun.*, 1, <https://doi.org/10.1088/2515-7620/ab2c65>, 2019.

523 Salzmann, M., Weser, H., Cherian, R.: Robust response of Asian summer monsoon to anthropogenic aerosols in  
524 CMIP5 models, *J. Geophys. Res. Atmos.*, 119, <https://doi.org/10.1002/2014JD021783>, 2014.

525 Salzmann, M., and Cherian, R.: On the enhancement of the Indian summer monsoon drying by Pacific  
526 multidecadal variability during the latter half of the twentieth century, *J. Geophys. Res. Atmos.*, 120,  
527 <https://doi.org/10.1002/2015JD023313>, 2015.

528 Samset, B. H., et al.: Climate impacts from a removal of anthropogenic aerosol emissions. *Geophys. Res. Lett.*,  
529 45, <https://doi.org/10.1002/2017GL076079>, 2018.

530 Samset, B.H., Lund, M.T., Bollasina, M., et al.: Emerging Asian aerosol patterns. *Nat. Geosci.*, 12,  
531 <https://doi.org/10.1038/s41561-019-0424-5>, 2019.

532 Schneider, U., Becker, A., Finger, P. et al.: GPCP's new land surface precipitation climatology based on quality-  
533 controlled in situ data and its role in quantifying the global water cycle, *Theor. Appl. Climatol.*, 115,  
534 <https://doi.org/10.1007/s00704-013-0860-x>, 2014,

535 Shao, Z., Wang, H., Geng, Y.F., et al.: East Asian summer monsoon response to anthropogenic aerosols  
536 redistribution: contrasting 1950–1980 and 1980–2010 to understand the role of non-Asian forcing, *Clim.*  
537 *Dynam.*, 62, <https://doi.org/10.1007/s00382-023-07016-x>, 2024.

538 Shawki, D., Voulgarakis, A., Chakraborty, A., Kasoar, M., and Srinivasan, J.: The South Asian monsoon response  
539 to remote aerosols: Global and regional mechanisms, *J. Geophys. Res.*, 123,  
540 <https://doi.org/10.1029/2018JD028623>, 2018.

541 Simpson, I. R., and Coauthors: The CESM2 single-forcing large ensemble and comparison to CESM1:  
542 implications for experimental design. *J. Climate*, 36, <https://doi.org/10.1175/JCLI-D-22-0666.1>, 2023.

543 Smith, S. J., van Aardenne, J., Klimont, Z., Andres, R. J., Volke, A., and Delgado Arias, S.: Anthropogenic sulfur  
544 dioxide emissions: 1850–2005, *Atmos. Chem. Phys.*, 11, <https://doi.org/10.5194/acp-11-1101-2011>, 2011.

545 Smith, D., Gillett, N. P., Simpson, I. R., Athanasiadis, P. J., Baehr, J., Bethke, I., et al.: Attribution of multi-annual  
546 to decadal changes in the climate system: The large ensemble single forcing model intercomparison project

547 (LESMIP), *Front. Clim.*, 4, <https://doi.org/10.3389/fclim.2022.955414>, 2022.

548 Song, F., Zhou, T., and Qian, Y.: Responses of East Asian summer monsoon to natural and anthropogenic forcings  
549 in the 17 latest CMIP5 models, *Geophys. Res. Lett.*, 41, <https://doi.org/10.1002/2013GL058705>, 2014.

550 Stier, P., van den Heever, S.C., Christensen, M.W., et al.: Multifaceted aerosol effects on precipitation, *Nat.*  
551 *Geosci.*, 17, <https://doi.org/10.1038/s41561-024-01482-6>, 2024.

552 Swapna, P., Krishnan, R., and Wallace, J.M.: Indian Ocean and monsoon coupled interactions in a warming  
553 environment, *Clim. Dynam.*, 42, <https://doi.org/10.1007/s00382-013-1787-8>, 2014.

554 Szopa, S., et al.: Short-Lived Climate Forcers. In *Climate Change 2021: The Physical Science Basis. Contribution*  
555 *of Working Group I to the Sixth Assessment Report of the Intergovernmental Panel on Climate Change*  
556 [Masson-Delmotte, V., P. Zhai, A. Pirani, S.L. Connors, C. Péan, S. Berger, N. Caud, Y. Chen, L. Goldfarb,  
557 M.I. Gomis, M. Huang, K. Leitzell, E. Lonnoy, J.B.R. Matthews, T.K. Maycock, T. Waterfield, O. Yelekçi, R.  
558 Yu, and B. Zhou (eds.)]. Cambridge University Press, Cambridge, United Kingdom and New York, NY, USA,  
559 pp. 817–922, <https://doi.org/10.1017/9781009157896.008>, 2021.

560 Takaya, K., and Nakamura, H.: A formulation of a phase-independent wave-activity flux for stationary and  
561 migratory quasigeostrophic eddies on a zonally varying basic flow, *J. Atmos. Sci.*, 58,  
562 [https://doi.org/10.1175/1520-0469\(2001\)058<0608:AFOAPI>2.0.CO;2](https://doi.org/10.1175/1520-0469(2001)058<0608:AFOAPI>2.0.CO;2), 2001.

563 Turner, A., and Annamalai, H.: Climate change and the South Asian summer monsoon, *Nature Clim. Change* 2,  
564 <https://doi.org/10.1038/nclimate1495>, 2012

565 Undorf, S., Bollasina, M., Booth, B., and Hegerl, G.: Contrasting the effects of the 1850-1975 increase in sulphate  
566 aerosols from North America and Europe on the Atlantic in the CESM, *Geophys. Res. Lett.*, 45,  
567 <https://doi.org/10.1029/2018GL079970>, 2018.

568 Undorf, S., Polson, D., Bollasina, M. A., Ming, Y., Schurer, A., and Hegerl, G. C.: Detectable impact of local and  
569 remote anthropogenic aerosols on the 20th century changes of West African and South Asian monsoon  
570 precipitation, *J. Geophys. Res.*, 123, <https://doi.org/10.1029/2017JD027711>, 2018.

571 Wang, Q., Wang, Z., and Zhang, H.: Impact of anthropogenic aerosols from global, East Asian, and non-East  
572 Asian sources on East Asian summer monsoon system, *Atmos. Res.*, 183,  
573 <https://doi.org/10.1016/j.atmosres.2016.08.023>, 2017.

574 Wang, B., and Coauthors: Toward predicting changes in the land monsoon rainfall a decade in advance. *J. Climate*,  
575 31, <https://doi.org/10.1175/JCLI-D-17-0521.1>, 2018.

576 Wang, Z., Mu, J., Yang, M., and Yu, X.: Reexamining the mechanisms of East Asian summer monsoon changes  
577 in response to non–East Asian anthropogenic aerosol forcing. *J. Climate*, 33, [https://doi.org/10.1175/JCLI-D-](https://doi.org/10.1175/JCLI-D-19-0550.1)  
578 [19-0550.1](https://doi.org/10.1175/JCLI-D-19-0550.1), 2020.

579 Wang, Z., Lin, L., Xu, Y., et al.: Incorrect Asian aerosols affecting the attribution and projection of regional climate  
580 change in CMIP6 models, *npj Clim. Atmos. Sci.*, 4, <https://doi.org/10.1038/s41612-020-00159-2>, 2021.

581 Wang, Z., Feng, J., Diao, C., Li, Y., Lin, L., and Xu, Y.: Reduction in European anthropogenic aerosols and the  
582 weather conditions conducive to PM<sub>2.5</sub> pollution in North China: a potential global teleconnection pathway,  
583 *Environ. Res. Lett.*, 16, <https://doi.org/10.1088/1748-9326/ac269d>, 2021.

584 Watanabe, M.: Asian jet waveguide and a downstream extension of the North Atlantic Oscillation, *J. Climate*, 17,  
585 <https://doi.org/10.1175/JCLI-3228.1>, 2004.

586 Westervelt, D. M., Conley, A. J., Fiore, A. M., Lamarque, J.-F., Shindell, D. T., Previdi, M., Mascioli, N. R.,  
587 Faluvegi, G., Correa, G., and Horowitz, L. W.: Connecting regional aerosol emissions reductions to local and  
588 remote precipitation responses, *Atmos. Chem. Phys.*, 18, 12461–12475, [https://doi.org/10.5194/acp-18-](https://doi.org/10.5194/acp-18-12461-2018)  
589 [12461-2018](https://doi.org/10.5194/acp-18-12461-2018), 2018.

590 Wilcox, L. J., Allen, R. J., Samset, B. H., Bollasina, M. A., et al.: The Regional Aerosol Model Intercomparison  
591 Project (RAMIP), *Geosci. Model Dev.*, 16, <https://doi.org/10.5194/gmd-16-4451-2023>, 2023.

592 Wilcox L. J., Liu, Z., Samset, B. H., et al.: Accelerated increases in global and Asian summer monsoon  
593 precipitation from future aerosol reductions, *Atmos. Chem. Phys.*, 20, [https://doi.org/10.5194/acp-20-11955-](https://doi.org/10.5194/acp-20-11955-2020)  
594 [2020](https://doi.org/10.5194/acp-20-11955-2020), 2020.

595 Willmott, C. J., and Matsuura, K.: Smart interpolation of annually averaged air temperature in the United States,  
596 *J. Appl. Meteor. Climatol.*, 34, [https://doi.org/10.1175/1520-0450\(1995\)034<2577:SIOAAA>2.0.CO;2](https://doi.org/10.1175/1520-0450(1995)034<2577:SIOAAA>2.0.CO;2),  
597 1995.

598 Wu, G. X., Li, Z. Q., Fu, C. B., Zhang, X. Y., Zhang, R. Y., Zhang, R. H., et al.: Advances in studying interactions  
599 between aerosols and monsoon in China. *Science China Earth Sciences*, 59, [https://doi.org/10.1007/s11430-](https://doi.org/10.1007/s11430-015-5198-z)  
600 [015-5198-z](https://doi.org/10.1007/s11430-015-5198-z), 2016.

601 Xiang, B., Xie, S. P., Kang, S. M. et al.: An emerging Asian aerosol dipole pattern reshapes the Asian summer  
602 monsoon and exacerbates northern hemisphere warming, *npj Clim. Atmos. Sci.*, 6,  
603 <https://doi.org/10.1038/s41612-023-00400-8>, 2023.

604 Xie, P., and Arkin, P. A.: Global precipitation: A 17-Year monthly analysis based on gauge observations, satellite

605 estimates, and numerical model outputs, *Bull. Amer. Meteor. Soc.*, 78, [https://doi.org/10.1175/1520-](https://doi.org/10.1175/1520-0477(1997)078<2539:GPAYMA>2.0.CO;2)  
606 [0477\(1997\)078<2539:GPAYMA>2.0.CO;2](https://doi.org/10.1175/1520-0477(1997)078<2539:GPAYMA>2.0.CO;2), 1997.

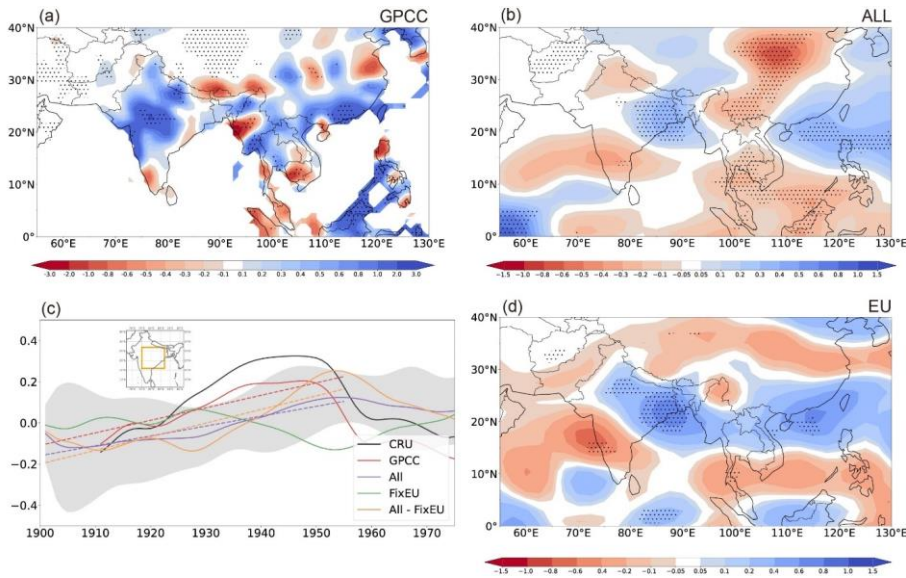
607 Zelinka, M. D., Andrews, T., Forster, P. M., and Taylor, K. E.: Quantifying components of aerosol-cloud-radiation  
608 interactions in climate models, *J. Geophys. Res. Atmos.*, 119, <https://doi.org/10.1002/2014JD021710>, 2014.

609 Zelinka, M. D., Smith, C. J., Qin, Y., and Taylor, K. E.: Comparison of methods to estimate aerosol effective  
610 radiative forcings in climate models, *Atmos. Chem. Phys.*, 23, <https://doi.org/10.5194/acp-23-8879-2023>,  
611 2023.

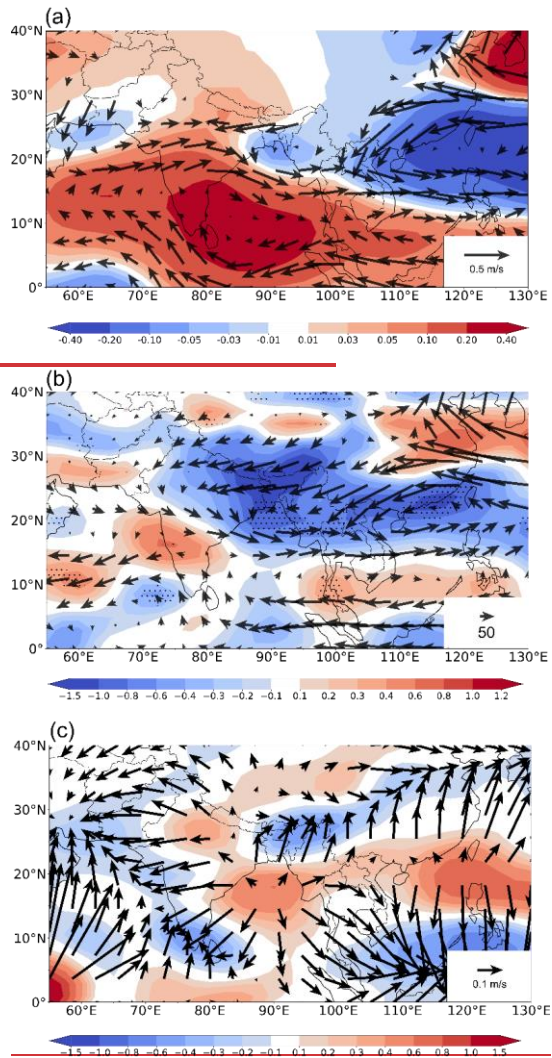
612 Zhang, L., and Zhou, T.: An assessment of monsoon precipitation changes during 1901–2001. *Clim. Dynam.*, 37,  
613 <https://doi.org/10.1007/s00382-011-0993-5>, 2011.

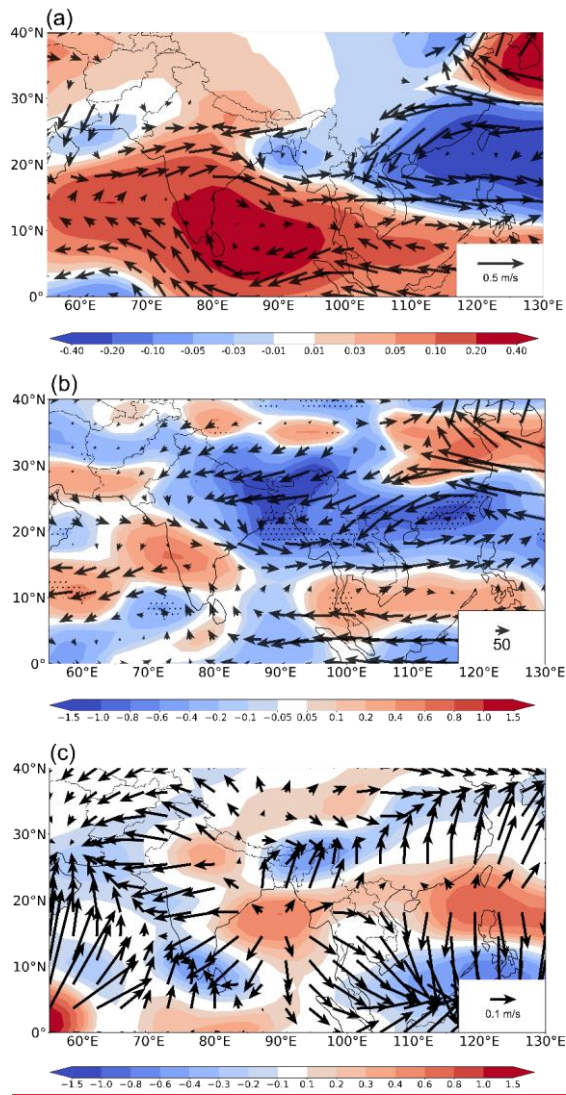
614

615 **Figures**  
616



617  
618  
619 **Figure 1.** (a)-(b): Spatial patterns of the 1901-1955 linear trends of JJA precipitation ( $\text{mm day}^{-1} (55 \text{ years})^{-1}$ ) for  
620 (a) GPCCC, (b) the all-forcing ensemble (ALL), and (d) the difference between ALL and the all-forcing experiment  
621 with fixed preindustrial aerosol emissions over Europe (fixEU), representing the impact of EU aerosols. The black  
622 dots mark the grid points for which the trend exceeds the 90% significance level according to the two-tailed  
623 Student's t-test. (c): Time series of area-averaged JJA precipitation anomalies ( $\text{mm day}^{-1}$ ; deviations from the  
624 1901-2000 climatology) over central-northern India (land-only points within  $75^{\circ}$ - $87^{\circ}$ E,  $16^{\circ}$ - $27^{\circ}$ N; area shown in  
625 inset map) smoothed with 11-year running means to highlight low-frequency (multi-decadal) fluctuations. The  
626 black and red lines represent observations (CRU and GPCCC, respectively), while the purple, green and orange  
627 lines represent the ensemble means of ALL, fixEU, and their difference (EU). The grey shading represents the  
628 standard deviation of the eight-member ALL ensemble around the mean. The 1901-1955 least-squares linear  
629 trends of the simulated time series are shown as dashed lines in the corresponding colours. Note that the interval  
630 for the simulated changes is half of that used for the observations.  
631  
632

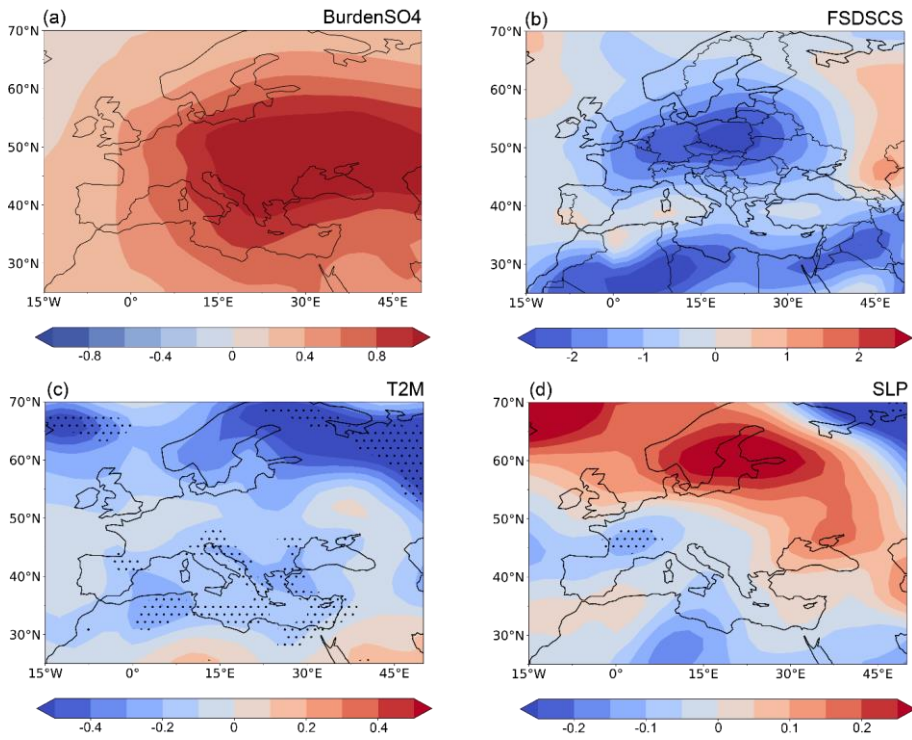




634

635 **Figure 2.** Spatial patterns of the 1901-1955 linear trends of the JJA average (a) 850-hPa winds ( $\text{m s}^{-1}$  (55 years)<sup>-1</sup>)  
 636 <sup>1</sup>) and 925-hPa streamfunction (colors,  $10^6 \text{ m}^2 \text{ s}^{-1}$  (55 years)<sup>-1</sup>), (b) 1000-300 hPa vertically integrated moisture  
 637 transport (vectors,  $\text{Kg m}^{-1} \text{ s}^{-1}$ ) and its divergence (shades,  $\text{mm d}^{-1}$  (55 years)<sup>-1</sup>), (c) 150-hPa divergent circulation  
 638 ( $\text{m s}^{-1}$  (55 years)<sup>-1</sup>) and its divergence (shades;  $10^6 \text{ s}^{-1}$  (55 years)<sup>-1</sup>) associated with increased European sulphate  
 639 aerosols (difference between the ALL and fixEU ensemble means). The black dots in (b) mark the grid points for  
 640 which the trend exceeds the 90% significance level according to the two-tailed Student's t-test.

641

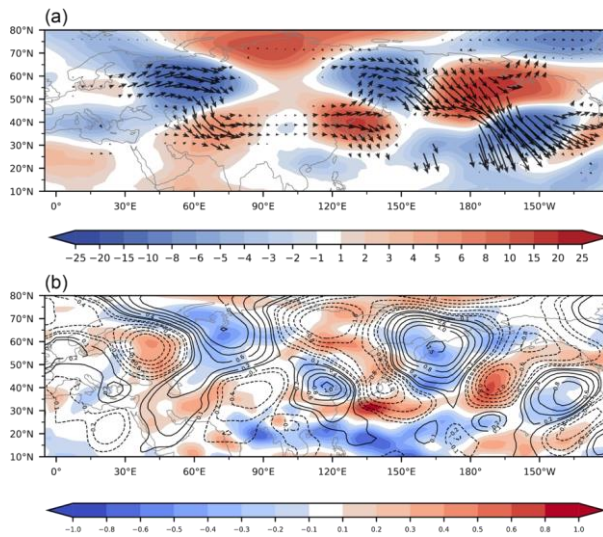


642

643

644 **Figure 3.** Spatial patterns of the 1901-1955 linear trends of the JJA average (a) column sulphate aerosol burden  
645 ( $10^{-5} \text{ kg m}^{-2} (55 \text{ years})^{-1}$ ), (b) surface clear-sky downward shortwave radiation ( $\text{W m}^{-2} (55 \text{ years})^{-1}$ ), (c) 2-m air  
646 temperature ( $\text{K} (55 \text{ years})^{-1}$ ), and (d) sea level pressure ( $\text{hPa} (55 \text{ years})^{-1}$ ) associated with increased European  
647 sulphate aerosols (difference between the ALL and fixEU ensemble means). The black dots in (c) and (d) mark  
648 the grid points for which the trend exceeds the 90% significance level according to the two-tailed Student's t-test.  
649

650



651  
652

653 **Figure 4.** Spatial patterns of the 1901-1955 linear trends of the JJA average (a) 300-hPa wave activity flux  
654 (vectors;  $10^{-4} \text{ m}^2 \text{ s}^{-2} (55 \text{ years})^{-1}$ ) and streamfunction (shades;  $10^6 \text{ m}^2 \text{ s}^{-1} (55 \text{ years})^{-1}$ ), and (b) 300-hPa meridional  
655 wind (contours;  $\text{m s}^{-1} (55 \text{ years})^{-1}$ ) and 500-hPa vertical velocity (shades;  $10^{-2} \text{ Pa s}^{-1} (55 \text{ years})^{-1}$ ) associated with  
656 increased European sulphate aerosols (difference between the ALL and fixEU ensemble means).